Article

One Scaffold, Two Conformations: The Ring-Flip of the Messenger InsP$_8$ Occurs under Cytosolic Conditions

Leonie Kurz [1,2] **, Peter Schmieder** [1] **, Nicolás Veiga** [3,*] **and Dorothea Fiedler** [1,2,*]

[1] Leibniz-Forschungsinstitut für Molekulare Pharmakologie, Robert-Rössle-Straße 10, 13125 Berlin, Germany
[2] Institut für Chemie, Humboldt-Universität zu Berlin, Brook-Taylor-Straße 2, 12489 Berlin, Germany
[3] Química Inorgánica, Departamento Estrella Campos, Facultad de Química, Universidad de la República (UdelaR), Av. Gral. Flores 2124, Montevideo 11800, Uruguay
[*] Correspondence: nveiga@fq.edu.uy (N.V.); fiedler@fmp-berlin.de (D.F.)

Abstract: Inositol poly- and pyrophosphates (InsPs and PP-InsPs) are central eukaryotic messengers. These very highly phosphorylated molecules can exist in two distinct conformations, a canonical one with five phosphoryl groups in equatorial positions, and a "flipped" conformation with five axial substituents. Using ^{13}C-labeled InsPs/PP-InsPs, the behavior of these molecules was investigated by 2D-NMR under solution conditions reminiscent of a cytosolic environment. Remarkably, the most highly phosphorylated messenger $1,5(PP)_2$-InsP$_4$ (also termed InsP$_8$) readily adopts both conformations at physiological conditions. Environmental factors—such as pH, metal cation composition, and temperature—strongly influence the conformational equilibrium. Thermodynamic data revealed that the transition of InsP$_8$ from the equatorial to the axial conformation is, in fact, an exothermic process. The speciation of InsPs and PP-InsPs also affects their interaction with protein binding partners; addition of Mg^{2+} decreased the binding constant K_d of InsP$_8$ to an SPX protein domain. The results illustrate that PP-InsP speciation reacts very sensitively to solution conditions, suggesting it might act as an environment-responsive molecular switch.

Keywords: InsP$_8$; inositol pyrophosphates; conformation; NMR; ring-flip; molecular switch; pH sensing; metal coordination

1. Introduction

Myo-inositol polyphosphates (InsPs) are a family of messenger molecules that control a wide array of biological processes in eukaryotic cells (Figure 1a). In these molecules, the phosphoryl groups are arranged in different numbers and patterns around the inositol scaffold, creating great structural variety that ranges from species with only one phosphoryl group to the inositol pyrophosphates (PP-InsPs), which carry seven or eight phosphates [1–3]. The PP-InsPs contain one or two high-energy diphosphate groups, in addition to monophosphates, thereby accommodating an extraordinary negative charge density.

The most highly phosphorylated PP-InsP in mammals is $1,5(PP)_2$-InsP$_4$, (from here on abbreviated as InsP$_8$), which is generated via the phosphorylation of 5PP-InsP$_5$ by PPIP5Ks (diphosphoinositol-pentakisphosphate kinases), or phosphorylation of 1PP-InsP$_5$ by IP6Ks (inositol hexakisphosphate kinases). In recent years, InsP$_8$ has emerged as a regulator of inorganic phosphate homeostasis in various organisms. The enzymatic activity of PPIP5Ks is directly regulated by phosphate concentrations, and cellular levels of InsP$_8$ correlate with phosphate availability [4,5]. In fission yeast (*S. pombe*), InsP$_8$ activates the vacuolar VTC complex by putatively binding to an SPX domain, driving polyphosphate synthesis to store excess phosphate [6]. In plants, it was demonstrated that the activity of the InsP$_8$-producing enzymes VIH1/2 negatively regulates phosphate starvation responses [7]. Mechanistically, InsP$_8$ binds to a standalone SPX domain (SPX1) in *A. thaliana*, which enables dimerization with the transcription factor PHR1 and suppresses downstream targets [8]. In cultured human cell lines, InsP$_8$ was found to activate phosphate efflux by binding to the SPX domain

of XPR1, removing excess phosphate and preventing tissue calcifications [9–11]. Moreover, at an organismal level, mutations in PPIP5Ks are associated with hearing loss [12,13].

The function of 5PP-InsP$_5$ has been investigated more closely, especially its role in cellular energy signaling, where the production of 5PP-InsP$_5$ critically depends on ATP levels and regulates glycolytic flux accordingly [14,15]. Notably, 5PP-InsP$_5$ stimulates exocytosis of insulin-containing granules from pancreatic β-cells, ostensibly by competing with the plasma membrane lipid phosphatidylinositol-4,5-bisphosphate (PIP$_2$) for binding of synaptotagmin 7 [16,17]. 5PP-InsP$_5$ also inhibits the activity of Akt kinase, a central metabolic regulator, by binding to the PH domain of Akt, releasing it from the plasma membrane, preventing its activation [18–20]. As a result, IP6K1 knockout mice display abnormally high Akt activity and are resistant to weight-gain when fed a high-fat diet [18]. IP6K1 knockout in mice also increases the activity of AMPK, inhibiting fat accumulation in favor of thermogenesis, and further supporting the lean phenotype [21].

In many cases it is difficult to attribute an observed phenotype to an individual messenger, because genetic deletion of IP6Ks inevitably reduces the levels of both 5PP-InsP$_5$ and InsP$_8$ [22]. Even when biochemical insight into the mechanisms of action is available, it sometimes cannot explain why PP-InsPs possess distinct biological functions, in spite of their close structural relatedness and similarly high charge density. For example, phosphate efflux via XPR1 is activated almost exclusively by InsP$_8$, even though 1PP-InsP$_5$ and 5PP-InsP$_5$ bind with similar dissociation constants (K$_d$) to the SPX domain [9]. Binding affinities are also similar for InsP$_8$ and 5PP-InsP$_5$ towards the SPX1 protein in rice (*O. sativa*), but genetic experiments have indicated that only InsP$_8$ is the physiologically relevant ligand [8]. Similarly, in in vitro experiments, InsP$_8$ is twenty-times more effective than 5PP-InsP$_5$ at activating polyphosphate synthesis by the VTC complex from budding yeast *S. cerevisiae*, despite a charge difference of only one. It was also more effective than other InsP$_8$ isomers [23], suggesting that affinity is determined by the exact shape of the molecule, rather than sheer charge density. In another example from fission yeast *S. pombe*, polyphosphate synthesis by the VTC complex clearly depended on InsP$_8$, synthesized by the PPIP5K orthologue Asp1 [6]. Possible explanations for how substrate specificity of PP-InsP-binding proteins may be regulated include ternary interactions with more than one binding partner, local production of individual PP-InsPs, and localized differences in solution conditions, which change protonation and metal complexation.

A property unique to highly phosphorylated InsPs is their ability to adopt an alternate conformation at elevated pH, where the substituent at the 2-position is equatorial, and all others are axial, which separates the phosphoryl groups further in space and reduces charge repulsion between them (Figure 1b,c) [24–27]. The PP-InsPs and their non-hydrolyzable methylene bisphosphonate analogs (PCP-InsPs, Figure 1b) also display this behavior, and appear to have a higher propensity to adopt the axial conformation relative to the InsPs, especially in the presence of magnesium cations [28].

PP-InsPs can potentially form a wide range of different species, depending on their conformation, protonation state and complexation of metal cations. We therefore wanted to obtain a more detailed understanding of PP-InsP speciation, specifically under conditions approximating a cytosolic setting. Due to the structural information it provides, NMR spectroscopy is the method of choice for characterizing these equilibria, but the lack of sensitivity has limited past investigations to experiments using non-physiological concentrations of InsPs and PP-InsPs (>100 μM) [28].
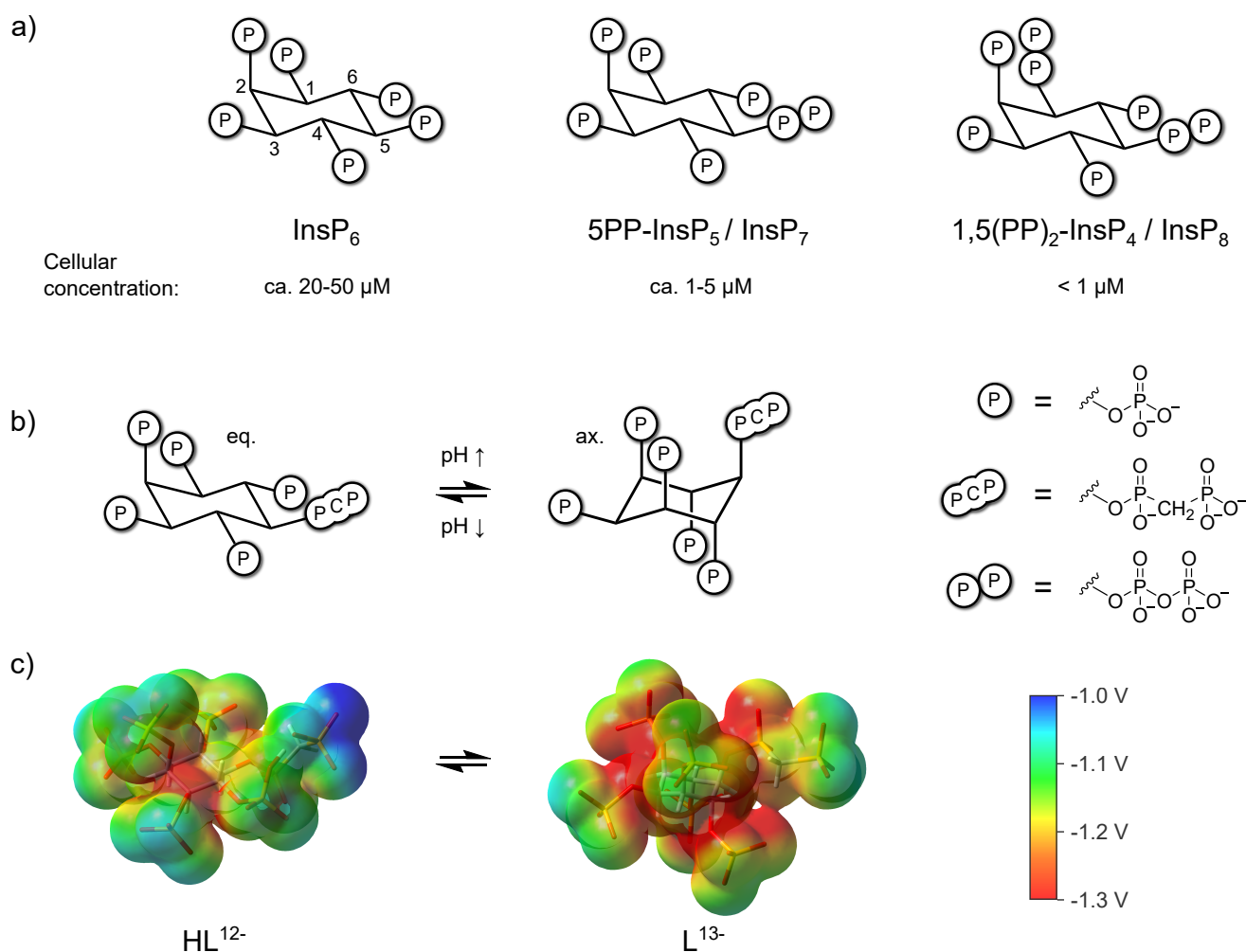
Figure 1. (**a**) Structure of $InsP_6$, $5PP\text{-}InsP_5$, $InsP_8$ and approximate concentrations in mammalian cells [29–32]. (**b**) pH-dependent equilibrium between axial (ax.) and equatorial (eq.) conformation of the non-hydrolyzable $5PP\text{-}InsP_5$ analogue $5PCP\text{-}InsP_5$ [28] (**c**) Electrostatic potential mapped on an isodensity surface for fully deprotonated, axial $5PCP\text{-}InsP_5$ (L^{13-}) and monoprotonated, equatorial $5PCP\text{-}InsP_5$ (HL^{12-}) (B3LYP/3-21 + G* geometries; isodensity value = 0.004, scale: −1.3 V (red) to −1.0 V (blue)). Atom color code: C (grey), H (white), O (red), P (orange).

Here, we have conducted a systematic comparison of $InsP_6$, $5PP\text{-}InsP_5$ and $InsP_8$ using NMR spectroscopy of ^{13}C-labeled compounds, to better understand the intricacies of their speciation. Intriguingly, we found that $InsP_8$ is able to adopt the axial conformation under conditions very reminiscent of a cytosolic environment. We then used ^{31}P-NMR to identify likely protonation states and K^+- and Mg^{2+}-complexes of $InsP_8$. Finally, ITC experiments revealed that addition of Mg^{2+} ions influenced the binding parameters of the interaction between $InsP_8$ and an SPX protein domain. Our results imply that conditions for biochemical and biophysical characterization of PP-InsP protein interactions should always be chosen with great care, and highlight $InsP_8$ as a potential pH-, metal ion-, and temperature-dependent intracellular molecular switch.

2. Materials and Methods

2.1. Synthesis and BIRD-HMQC NMR Analysis of InsPs

^{13}C-labeled InsPs and PP-InsPs were synthesized chemo-enzymatically, as previously published, with slight adjustments [30,33]. Enzymatic synthesis of $InsP_8$ was carried out at pH 6.0 instead of 6.4, and in the presence of additional 150 mM $(NH_4)_2SO_4$.

Samples for HMQC-NMR studies contained 50 μM $^{13}C_6$-labeled InsPs (InsP$_6$/5PP-InsP$_5$/InsP$_8$), 2 mM bis-tris-propane, 130 mM KCl, 10 mM NaCl and 0/50/250 μM MgCl$_2$ in D$_2$O.

BIRD-HMQC NMR spectra were recorded at 277 K and 600 MHz (^{1}H frequency) on a Bruker AV-III NMR spectrometer (Bruker Biospin, Rheinstetten, Germany) using cryogenically cooled 5 mm QCI-triple resonance probe equipped with one-axis self-shielded gradients. The spectrometer was operated using topspin 3.5 pl6 software. Instrument temperature was calibrated against $_4$-methanol according to Findeisen et al. [34]. Acquisition parameters were SW(^{13}C): 60–90 ppm, NS: 128, TD(^{13}C): 64.

2.2. Assignment of HMQC-NMR Spectra of Axial Conformations

BIRD-HMQC spectra were recorded at 277 K as described above, with samples containing 200 μM InsPs, 130 mM KCl, 10 mM NaCl, 2mM BTP in D$_2$O. pH was set to pH* 9.5 for InsP$_6$, pH* 8.8 for 5PP-InsP$_5$ and pH* 8.5 for InsP$_8$ (pH = 0.929 × pH* + 0.42 [35]). NOESY-HMQC spectra of the same samples were subsequently recorded using mixing times of 80 ms for InsP$_6$ and 5PP-InsP$_5$ and 200 ms for InsP$_8$. Conformational exchange on the time-scale of the experiment created cross-peaks between corresponding peaks in different conformations, which allowed us to assign each peak of the equatorial conformer to its axial counterpart.

2.3. Van't Hoff Thermodynamic Analysis

BIRD-HMQC NMR spectra were recorded as described above, at 274–283 K in 1 K steps, two replicate samples per condition. Instrument temperature was calibrated against d$_4$-methanol according to Findeisen et al. [34].

Samples contained 50 μM InsP$_8$, 5 mM HEPES pH* 7.5 (pH set on ice), 130 mM KCl, 10 mM NaCl, and either 100 μM or 250 μM MgCl$_2$. Acquisition parameters were SW(^{13}C): 62–82 ppm, NS: 2048, TD(^{13}C): 16.

The best-isolated peaks (the 2-peak of ax. and 1-peak of eq. conformer) were integrated, subtracting 1PP-InsP$_5$ impurities. The ax./eq. ratio (i.e., equilibrium constant K for the eq. to ax. transition) was plotted against 1/T, where T is temperature in Kelvin.

ΔH^0 and ΔS^0 were calculated from the regression line. Two replicates were combined for the linear regression.

2.4. NMR Titrations

In order to create a system free of coordinating counterions, a batch of InsP$_8$ was synthesized as described above, by enzymatic phosphorylation of 5PP-InsP$_5$ and precipitation with Mg^{2+}, followed by Mg^{2+} chelation on Amberlite$^®$ cation exchange resin. Unlike in the standard procedure, the resin was loaded with NMe$_4$Cl instead of NH$_4$CO$_3$, resulting in a batch of InsP$_8$ with non-coordinating NMe$_4^+$ counterions. 1 mM EDTA was added to all ^{31}P-NMR titrations to chelate remaining traces of Mg^{2+}.

NMR-samples contained 1 mM InsP$_8$, 1 mM EDTA, pH 3.0–12.5 (in H$_2$O, steps of 0.5 pH units) and a) for the non-coordinating condition: 150 mM NMe$_4$Cl or b) 150 mM KCl or c) 150 mM KCl and 1 mM MgCl$_2$. Sealed glass capillaries containing 50 mM phosphonoacetic acid in D$_2$O were added into the sample tubes for locking and chemical shift calibration.

^{31}P-NMR spectra were recorded at 295 K on a Bruker spectrometer (see above) operating at 600 MHz for protons and 244 MHz for phosphorous nuclei. SW: −40 ppm to −20 ppm, NS: 1024. Spectra at pH 3.0 were assigned by various 2D-NMR methods (Figure S5) and chemical shift changes were tracked across the pH range.

The data were analyzed using the HypNMR 2006 software (Hyperquad Limited, Lincoln, UK) [36]. Different possible stoichiometries were tested, and the final chemical models were selected on the basis of the σ parameter (scaled sum of square differences between predicted and experimental chemical shift values), the model confidence level estimator (chi square), and the internal consistency of data reflected in standard deviations

of the formation constants [37]. Species distribution diagrams were produced using the HySS program (Hyperquad Limited, Lincoln, UK) [38].

2.5. Isothermal Titration Calorimetry

The VTC2 SPX domain (residues 1–182) was expressed with a C-terminal His$_6$-tag and purified by Ni-affinity and size-exclusion chromatography, as previously published [39].

Protein stocks were diluted to 300 µL with final buffer conditions: 25 mM HEPES pH 7.4, 150 mM KCl, 40 mM NaCl, 0.5 mM TCEP (ITC buffer). The exact protein concentration for each replicate was determined separately by Bradford assay. InsP$_8$ was diluted to 500 µM in ITC buffer. For binding experiments in the presence of magnesium ions, both dilution buffers were supplemented with MgCl$_2$ to give a final concentration of 1 mM after dilution.

ITC experiments were carried out at 25 °C in a MicroCal PEAQ-ITC calorimeter (Malvern Panalytical GmbH, Kassel, Germany), with ca. 50 µM protein in the cell and 500 µM ligand in the syringe. InsP$_8$ was titrated into the solution in nineteen 2 µL-steps. Spacing between injections was 150 s.

The corresponding instrument software (MicroCal PEAQ-ITC Analysis) was used for baseline correction, peak integration, data fitting and determination of binding parameters.

2.6. DFT Calculations

The input geometries were built employing the protonation and complexation patterns determined by ^{31}P NMR in this report. Three water molecules were included in the first coordination sphere of the Mg^{2+} cation. The initial geometries were pre-optimized by means of a molecular mechanic method (MM+), in order to explore the potential energy surface. Then, a Density Functional Theory (DFT) optimization protocol was performed in Gaussian 09 (Gaussian Inc., Wallingford CT, USA) [40], using the B3LYP functional, with an ultrafine integration grid and the 3–21 + G* split valence basis set. The potassium ions were treated using the effective core potential LANL2DZ relativistic procedure [41]. The solvent was modelled through the Truhlar and coworkers' SMD solvation model [42]. All final structures were minima in the potential energy surface, being the nature of the stationary points verified through vibrational analysis.

3. Results

3.1. ^{1}H,^{13}C-HMQC NMR Spectra of PP-InsPs Can Show Two Conformations Simultaneously

The recent development of enzymatic syntheses for inositol pyrophosphates provides access to ^{13}C-labeled PP-InsPs at the scale of hundreds of micromoles [30,33]. The uniformly labeled PP-InsPs can readily be detected at concentrations below 50 µM in ^{1}H,[13]C HMQC experiments, which motivated us to systematically investigate InsP$_6$/PP-InsP speciation and conformation under different conditions, near physiological concentrations.

A ^{1}H,^{13}C HMQC NMR spectrum of InsP$_6$ (50 µM, no coordinating counter ions present) at pH* 6.5 (pH* = apparent pH in D$_2$O [35]; pH* 6.50 = pH 6.46) displayed four peaks due to the molecule's plane of symmetry, and was assigned to correspond to the equatorial conformation of InsP$_6$ (five phosphoryl groups in equatorial position, position 2 in axial position). An equivalent sample at pH* 12.0 displayed a different set of four peaks, shifted upfield in the carbon dimension, which corresponds to the axial conformation of InsP$_6$ (five phosphoryl groups axial, position 2 is equatorial) [43,44].

Unfortunately, when recording spectra at 37 °C, we noticed NMR-peak broadening, making detection of InsP$_6$ conformers impossible in a certain pH-range. This intermediate exchange effect had been observed before and impedes direct observation of InsPs/PP-InsPs by proton-based NMR methods near the conformational transition [26,28]. We therefore attempted to slow down exchange rates by cooling the sample and recording spectra at 4 °C. An HMQC-spectrum at 4 °C and pH* 9.0 (=pH 8.8) displayed signals of both the axial and the equatorial conformer simultaneously (Figure 2a).
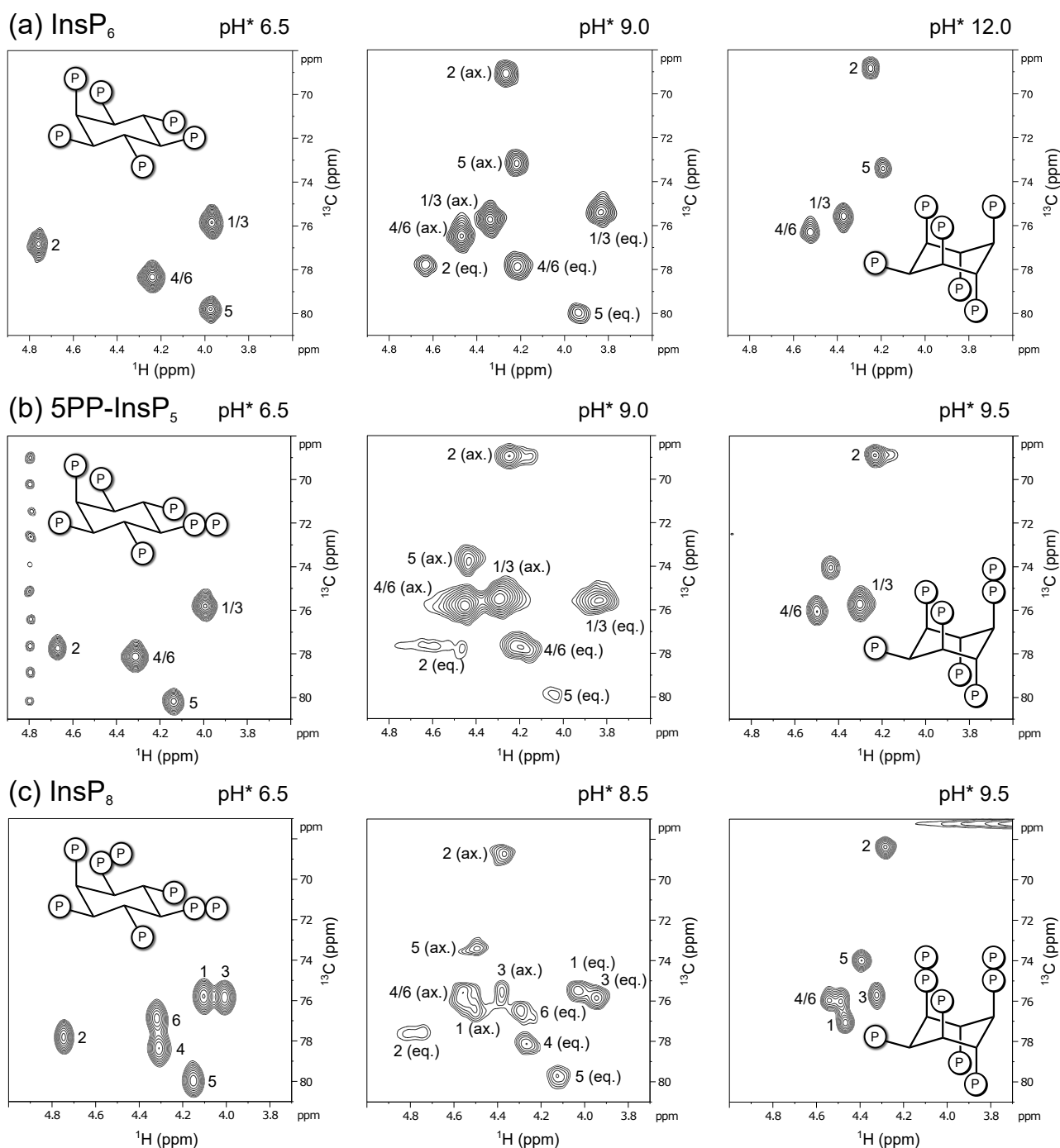
Figure 2. Representative ^{1}H,^{13}C-HMQC-NMR spectra of ^{13}C-labeled (**a**) InsP$_6$, (**b**) 5PP-InsP$_5$ and (**c**) InsP$_8$ in equatorial (eq.), axial (ax.) or mixed conformation, recorded at 4 °C. Peaks correspond to inositol backbone protons and are labeled according to their position in the myo-inositol ring. Samples contained 50 μM InsPs and 130 mM KCl, 10 mM NaCl in D$_2$O. pH*-values measured in D$_2$O can be converted to pH using the following formula: pH = 0.929 × pH* + 0.42 [35].

Concurrent observation of both conformations was also possible for the inositol pyrophosphates 5PP-InsP$_5$ and InsP$_8$ at 4 °C (Figure 2b,c). All HMQC–NMR peaks of IP$_6$ and the PP-InsPs in the axial conformation were assigned using a NOESY–HMQC–NMR method, which creates cross-peaks between corresponding peaks of the two conformations (Figure S1). These assignments allowed us to use integration to quantify the relative proportions of the two conformers.

3.2. Conformational Equilibria of InsP$_6$ and PP-InsPs Are Sensitive to pH and Ionic Composition

With the ability to detect and quantify both conformations over a wide pH range, at low InsP/PP-InsP concentrations, we sought to systematically compare the behavior of InsP$_6$, 5PP-InsP$_5$ and InsP$_8$, and characterize the influence of pH and biologically relevant metal ions on their conformation. We decided to maintain physiological concentrations of K$^+$ and Na$^+$ ions, while varying pH and concentration of the divalent cations Mg^{2+} and Ca^{2+}.

Since inositol polyphosphates are prone to precipitation in the presence of divalent metal ions, especially at basic pH, we wanted to ensure that this phenomenon did not perturb our analysis. In the presence of 5 equiv. Mg^{2+}, all three molecules showed notable precipitation within 24 h at pH* 9.0, but not at pH* 8.0 and lower (Figure S2).

Without divalent cations present, InsP$_6$ remained in its equatorial conformation over most of the observed pH range (6.5–9.5). Only when pH* was increased to 9.0 did traces of the axial conformer begin to appear, and even at pH* 9.5, less than half of InsP$_6$ was in the axial conformation (Figure 3a). The proportion of the axial conformer was increased by addition of Mg^{2+} cations. Addition of one equivalent was enough to shift the equilibrium to about 30% axial conformer at pH 9.0* and 90% axial conformer at pH* 9.5. Addition of five equivalents of Mg^{2+} facilitated the transition to the axial conformer even more (Figure 3a). Similar results were obtained when adding Ca^{2+} (Figure S3). These observations are consistent with previous reports that an elevation of pH and addition of metal cations can increase the proportion of the axial conformer [26,28,45].

For 5PP-InsP$_5$, without divalent cations present, about 10% axial conformer were already detected at pH* 8.5. At pH* 9.5, 5PP-InsP$_5$ was only detected in the axial conformation (Figure 3b). Like InsP$_6$, the proportion of 5PP-InsP$_5$ in the axial conformation was increased upon addition of Mg^{2+} ions. In the presence of five equivalents Mg^{2+}, 5PP-InsP$_5$ adopted exclusively the axial conformation at pH* 8.5 (=pH 8.3) and higher (Figure 3b). The effect of Ca^{2+} was slightly less pronounced. About 60% of 5PP-InsP$_5$ were in an axial conformation at pH* 8.5 in the presence of 5 equiv. Ca^{2+} (Figure S3).

The trend that transition to the axial conformation was facilitated by additional phosphoryl groups continued for InsP$_8$. Even without divalent cations present, about half of the molecules adopted the axial conformation at pH* 8.5 (Figure 3c). The addition of Mg^{2+} ions again further shifted the conformational equilibrium towards the axial conformation. With one equivalent of Mg^{2+}, about 10% of InsP$_8$ were in the axial conformation at pH* 7.5 (=pH 7.4). Upon addition of five equivalents of Mg^{2+}, InsP$_8$ was almost equally distributed between its axial and equatorial forms at pH* 7.5. This last result is particularly interesting, because it suggests that a substantial portion of InsP$_8$ can adopt the axial conformation under cytosolic conditions. Again, the effect of Ca^{2+} was similar but slightly weaker. About 15% of InsP$_8$ adopted the axial conformation at pH* 7.5 with 5 equiv. Ca^{2+}.

In sum, the characterization of InsP$_6$ and PP-InsPs using ^{1}H,^{13}C-HMQC NMR was consistent with previous observations: The proportion of axial conformer rises with increasing pH and elevated concentrations of divalent cations. Moreover, the more densely phosphorylated the InsP/PP-InsP, the lower the pH at which the molecule begins to transition to the axial conformation. Each successive phosphorylation decreases the pH value for the transition by roughly 0.5 pH units. Intriguingly, InsP$_8$ seems to undergo the conformational change at physiological pH and ionic composition, which prompted us to investigate this messenger molecule in more detail.
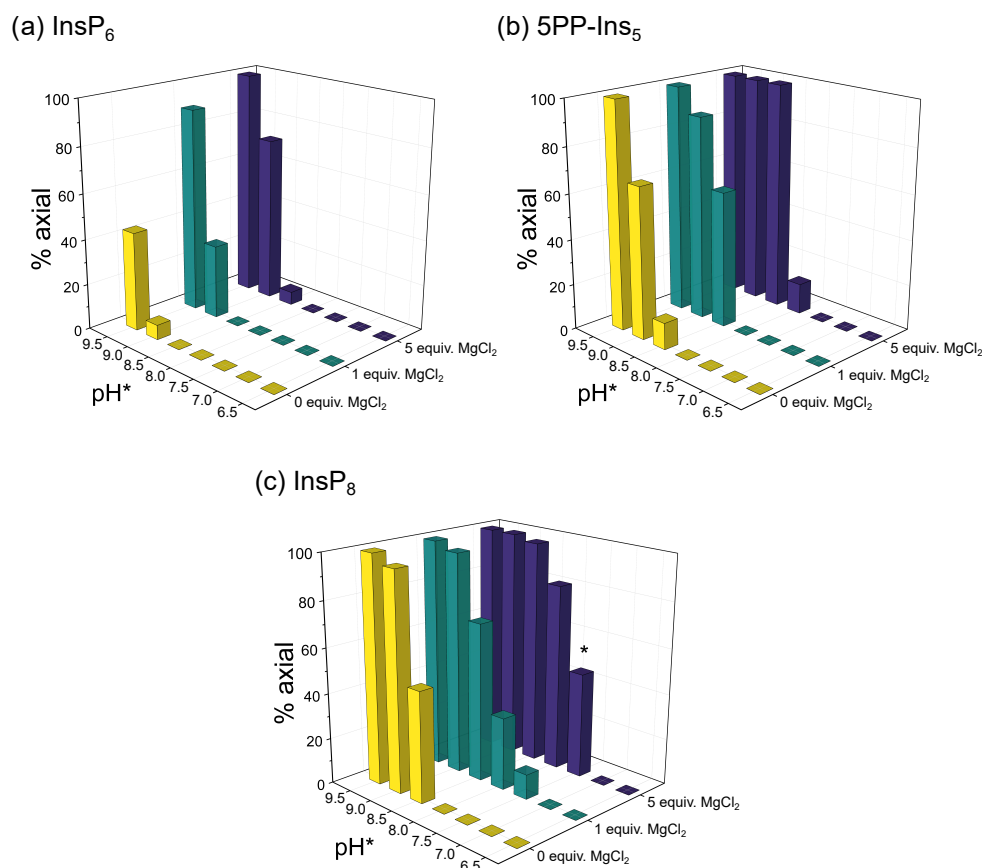
(a) InsP$_6$

(b) 5PP-Ins$_5$

(c) InsP$_8$

Figure 3. Relative abundance of (**a**) InsP$_6$, (**b**) 5PP-InsP$_5$ and (**c**) InsP$_8$ in axial conformation at different pH and 50 μM total InsP concentration in the presence of 0/1/5 equivalents MgCl$_2$ and physiological background of 130 mM KCl and 10 mM NaCl. ^{1}H,^{13}C-HMQC-NMR spectra were measured at 4 °C and integrated to obtain the ratio of eq. to ax. conformation. The proportion of ax. InsPs increases with pH, Mg^{2+} concentration and phosphorylation state (InsP$_6$ < 5PP-InsP$_5$ < InsP$_8$). Intriguingly, about half of InsP$_8$ molecules are in ax. conformation at physiological pH in the presence of five equivalents MgCl$_2$ (bar marked with *). To enable NMR detection, all samples were made up in D$_2$O. pH*-values measured in D$_2$O can be converted to pH using the following formula: pH = 0.929 × pH* + 0.42 [35]. Peaks of both conformations were integrated to obtain the relative abundance of axial vs. equatorial conformer.

3.3. InsP$_8$ Is Present in Both Conformations under Near-Physiological Conditions

To gain a deeper understanding of the forces governing the InsP$_8$ conformational equilibrium under near-physiological conditions, we wanted to evaluate what proportion of axial conformer might be present at 37 °C, by determining the thermodynamic parameters of the conformational equilibrium (Figure 4a). To do so, we recorded HMQC-NMR spectra (50 μM InsP$_8$, pH* 7.5, 130 mM KCl, 10 mM NaCl, 100 μM/250 μM MgCl$_2$) over a temperature range of 10 K and measured the amounts of the two conformers via integration. It was not possible to use a wider temperature range, due to the peak broadening described above, and the necessity to detect both conformations. The values for ΔH^0 and ΔS^0 were extracted from slope and intercept of the van't Hoff plots (Figure 4c,d). To assess the influence of Mg^{2+} ions, we measured two replicates with 2 equiv. and two replicates with 5 equiv. Mg^{2+}, keeping all other parameters constant. To avoid precipitation, the Mg^{2+} concentration could not be increased any further, although the excess of Mg^{2+} ions is much higher in cells. Similarly, InsP$_8$ could not be decreased to physiological concentrations of <1 μM without compromising the NMR detection.
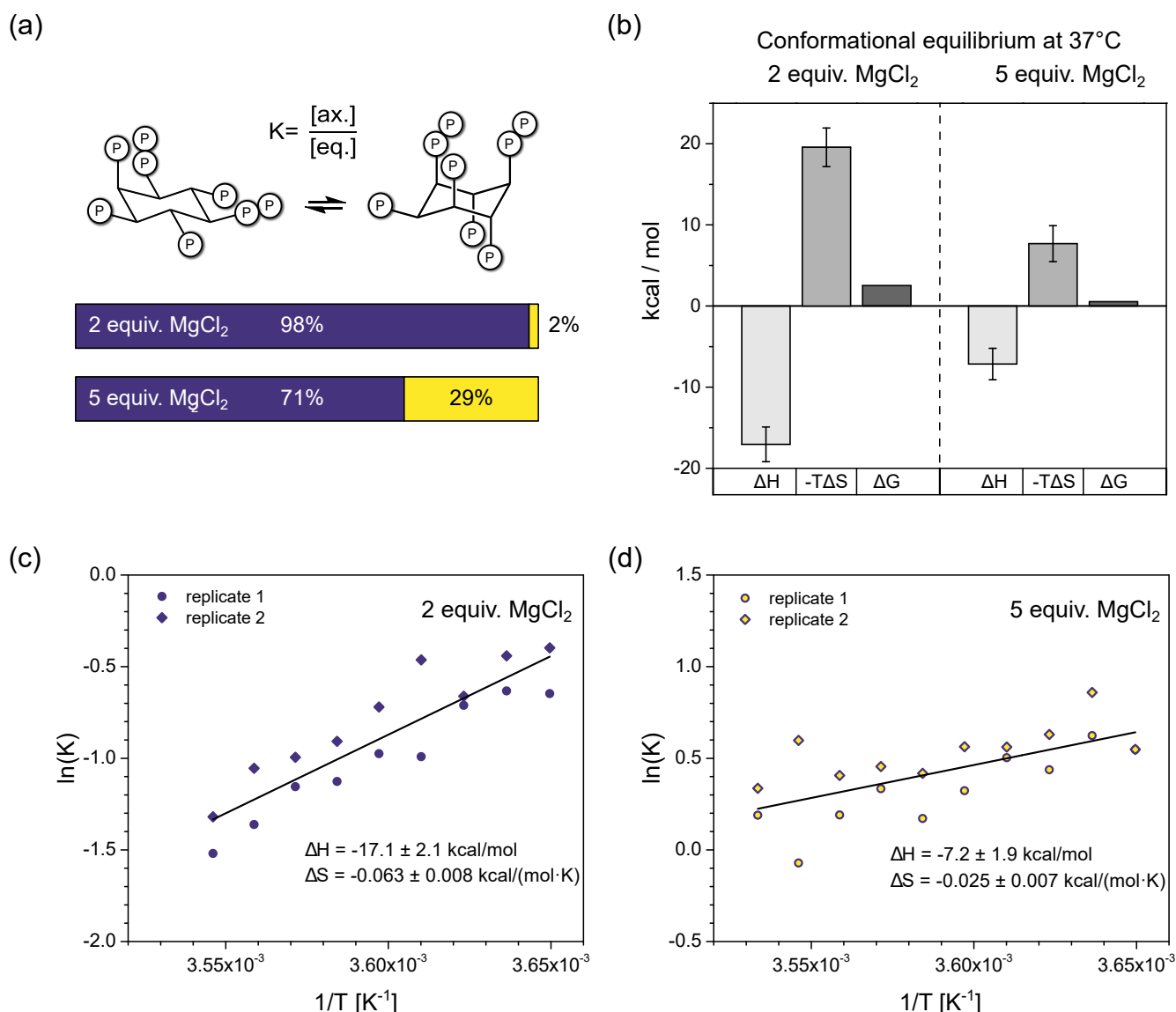
(a)

(b)

(c)

(d)

Figure 4. Thermodynamic analysis of InsP$_8$ conformational equilibrium. (**a**) Proportions of axial vs. equatorial conformer in the presence of 2 equiv. vs. 5 equiv. Mg^{2+}, according to Gibbs-Helmholtz equation and thermodynamic parameters from (**b**). (**b**) Results of van't Hoff analysis. Transition from eq. to ax. conformation is an exothermic process. While both entropic and enthalpic contributions are decreased by additional Mg^{2+}, overall, the equilibrium is shifted toward ax. conformation. (**c,d**) Van't Hoff plots of InsP$_8$ conformational equilibrium at pH 7.4 in the presence of (**c**) two equivalents, (**d**) five equivalents MgCl$_2$ and physiological background of 130 mM KCl and 10 mM NaCl. Temperature range: 274–283 K. ^{1}H,^{13}C-HMQC-NMR spectra were integrated to obtain the ratio of eq. to ax. conformer, i.e., the equilibrium constant K of the conformational equilibrium. Two replicates were treated as one for the linear regression. Thermodynamic parameters are reported ± standard error of regression.

In the presence of two equivalents of Mg^{2+}, the equilibrium seems to be governed by a balance of enthalpic gains and entropic losses upon transition to the axial conformation (Figure 4b), with $\Delta H^0 = -17.1 \pm 2.1$ kcal/mol and $\Delta S^0 = -0.063 \pm 0.008$ kcal/(mol·K). Somewhat unexpectedly, the equatorial to axial transition of InsP$_8$ is an exothermic process and the axial conformer is enthalpically more favorable. Using these thermodynamic values in the Gibbs-Helmholtz equation, we can estimate that at 37 °C, about 2% of InsP$_8$ would adopt an axial conformation under these solution conditions.

With five equivalents Mg^{2+} present, the equatorial to axial transition was again an exothermic process, with $\Delta H^0 = -7.2 \pm 1.9\,kcal/mol$ and $\Delta S^0 = -0.025 \pm 0.007\,kcal/(mol \cdot K)$. These values predict 29% axial conformer at 37 °C (310 K). Compared to the experiment with 2 equiv. $MgCl_2$, both ΔH^0 and ΔS^0 were reduced in magnitude by more than half. The relative change of ΔS^0 was larger, resulting in a net shift toward the axial conformation (Figure 4a,b).

In sum, our results suggest that substantial amounts of axial $InsP_8$ could be formed under cytosolic conditions, and that the conformational equilibrium is largely governed by entropic effects.

3.4. InsP8 Forms Strong Complexes with Potassium and Magnesium Ions

Given the unexpected thermodynamic parameters for the conformational equilibrium, we next wanted to characterize the protonation sequence and metal complexation of $InsP_8$ in solution. We utilized ^{31}P NMR for detection, because ^{31}P-NMR chemical shifts are very sensitive to both protonation and metal complexation, shifting upfield with each protonation step and downfield upon metal complexation [26,28,45]. The lower Larmor frequency of ^{31}P compared to ^{1}H allows detection of peaks which are broadened in ^{1}H NMR due to intermediate exchange phenomena.

^{31}P-NMR peaks were assigned to the eight phosphate groups (P1α, P1β, P2, P3, P4, P5α, P5β, P6) using a combination of 2D-NMR techniques (Figure S5). Titrations were performed at 1 mM $InsP_8$ concentration in the pH-range 3.0–12.5 under three different conditions: (i) without coordinating cations, where ionic strength and pH were maintained with NMe_4Cl/NMe_4OH (Figure 5a), (ii) with 150 mM KCl (Figure 5b) and (iii) with 150 mM KCl and 1 mM $MgCl_2$ (Figure 6a).

Under non-coordinating conditions, all signals shifted upfield with decreasing pH, as has been observed for $InsP_6$ and 5PCP-$InsP_5$ before (Figure 5a) [26,28]. Using HypNMR software, the experimental chemical shift values δ_P were fitted to generate a model of the protonation process and extract the first eight protonation constants of $InsP_8$, starting from the fully deprotonated molecule (L^{14-}, Table 1) [36]. Compared to $InsP_6$ and 5PCP-$InsP_5$, protonation constants were generally larger (indicating a greater proportion of protonated versus deprotonated state), presumably due to the higher negative charge of $InsP_8$, which stabilizes higher protonation states. The optimized chemical model indicated that H_5L^{9-} is the most abundant protonation state in the physiological pH range (Figures 5c and S6). Based on the calculated protonation constants, theoretical δ_P values could be calculated, which were in excellent agreement with the experimental values. The theoretical δ_P values and protonation constants could then be used to determine $\Delta\delta_P$ values (changes of theoretical δ_P with each successive protonation step, Table S1). Knowing that protonation causes an upfield shift, the $\Delta\delta_P$ values revealed the most likely protonation sites and sequence of protonation events (Figure S6). For example, during the first protonation step, the most negative $\Delta\delta_P$ values were observed for P3, P5β and P1β, suggesting that P3 shares its proton with P5β or P1β. Sudden chemical shift changes of all four monophosphate signals at around pH 11 indicated the conformational change (Figure 5a). Without coordinating cations present, the conformational change thus coincided with the second protonation step (for a full description of the analysis, see Supplementary Materials).
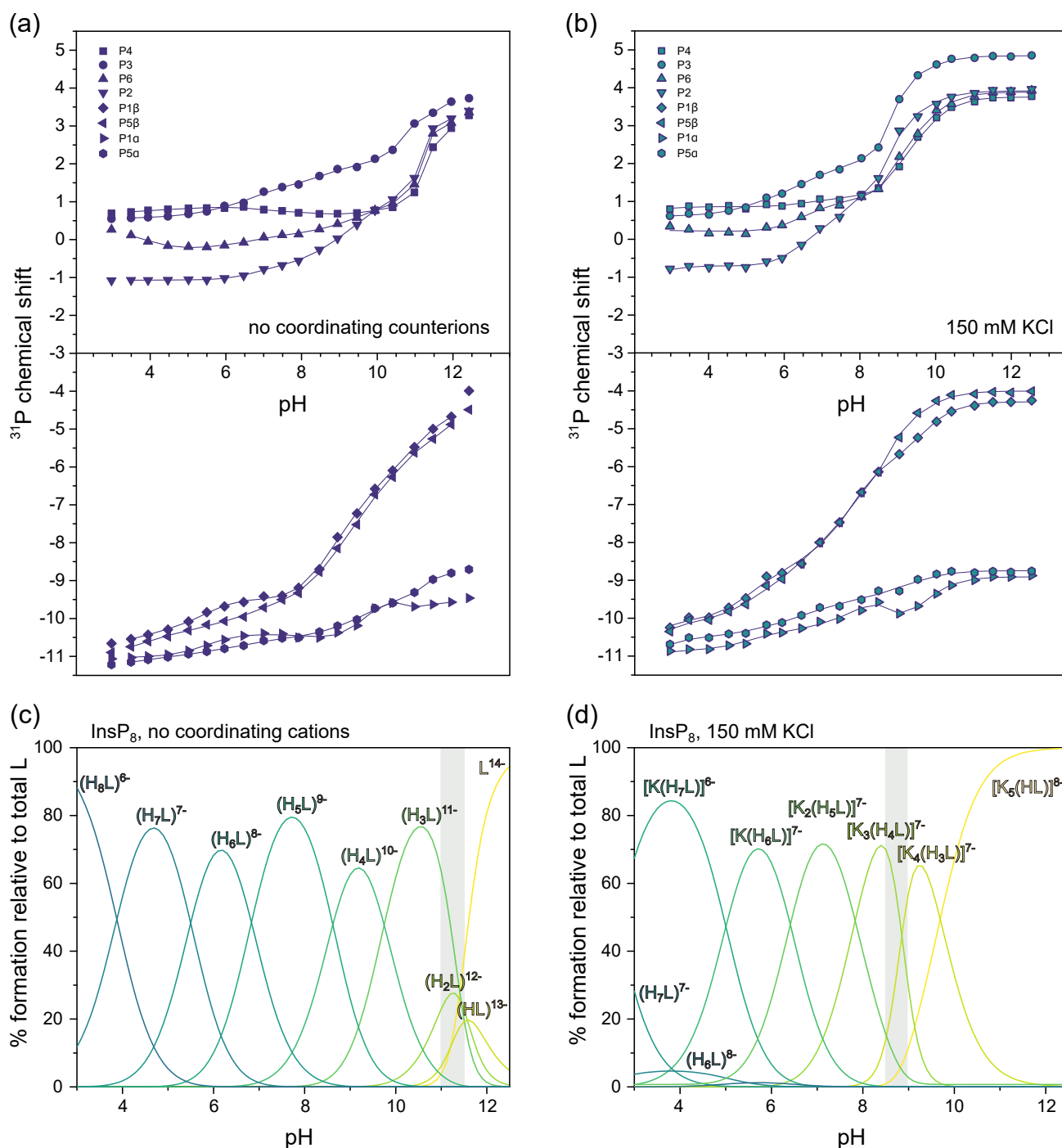
Figure 5. ^{31}P-NMR titrations of InsP$_8$. (**a**) Chemical shift without coordinating counterions (150 mM NMe$_4$Cl) at 22 °C, pH 3.0–12.5. (**b**) Chemical shift with 150 mM KCl. Dots represent experimental chemical shift data, separated into monophosphate (position 2, 3, 4, 6) and pyrophosphate groups (position 1 and 5). Lines represent theoretical chemical shift values based on the protonation model and calculated protonation constants. (**c**,**d**) Abundance of different protonation states (no coordinating counterions) or K$^+$-complexes (in the presence of 150 mM KCl) of InsP$_8$ (L) over the pH range. The grey area represents the pH-range with the biggest chemical shift changes in (**a**,**b**).
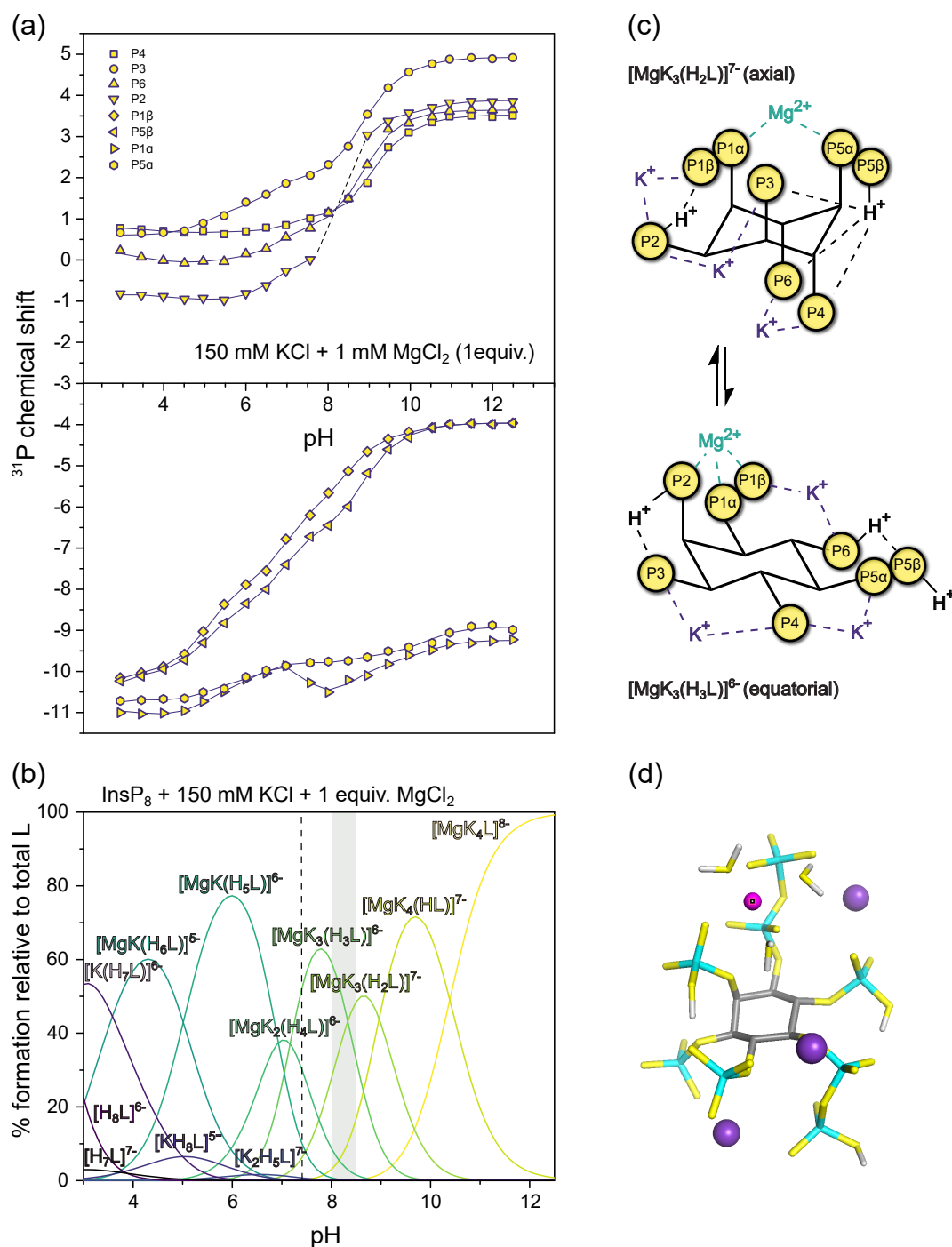
Figure 6. ^{31}P-NMR titrations of InsP$_8$. (**a**) Chemical shift with 150 mM KCl and 1 mM MgCl$_2$ at 22 °C, pH 3.0–12.5. Dots represent experimental chemical shift data, separated into monophosphate (position 2, 3, 4, 6) and pyrophosphate groups (position 1 and 5). Lines represent theoretical chemical shift values based on the protonation model and calculated protonation constants. (**b**) Abundance of different or K$^+$-Mg^{2+}-complexes (in the presence of 150 mM KCl) of InsP$_8$ (L) over the pH range. pH 7.4 is indicated by a dashed line. The grey area represents the pH-range with the biggest chemical shift changes in a. (**c**) Schematic view of the highest protonated axial and the lowest protonated equatorial complexes [MgK$_3$(H$_2$L)]$^{7-}$ and [MgK$_3$(H$_3$L)]$^{6-}$ (**d**) DFT optimized structure of the most abundant complex at pH 7.4, [MgK$_3$(H$_3$L)]$^{6-}$.

Table 1. Logarithms of the protonation and formation constants of InsP$_8$ (I = 0.15 M; T = 22 °C).

Equilibrium	log K		
	InsP$_8$	5PCP-InsP$_5$	InsP$_6$
	^{31}P NMR (22 °C) [a]	^{31}P NMR (22 °C) [b]	Potentiometry (37 °C) [b]
L^{14-} + H$^+$ ↔ HL^{13-}	11.21(1)	11.48(1)	10.8(1)
L^{14-} + 2 H$^+$ ↔ H$_2$L^{12-}	22.78(2)	22.42(2)	21.3(1)
L^{14-} + 3 H$^+$ ↔ H$_3$L^{11-}	34.22(2)	32.26(2)	31.63(6)
L^{14-} + 4 H$^+$ ↔ H$_4$L^{10-}	43.96(2)	40.94(2)	40.42(6)
L^{14-} + 5 H$^+$ ↔ H$_5$L^{9-}	52.58(3)	47.67(2)	47.32(6)
L^{14-} + 6 H$^+$ ↔ H$_6$L^{8-}	59.41(8)	51.93(2)	53.04(7)
L^{14-} + 7 H$^+$ ↔ H$_7$L^{7-}	64.91(6)	55.64(2)	56.14(9)
L^{14-} + 8 H$^+$ ↔ H$_8$L^{6-}	68.79(7)	—	—
5 K$^+$ + HL^{13-} ↔ [K$_5$(HL)]$^{8-}$	12.47(3)	6.57(3)	—
4 K$^+$ + H$_2$L^{12-} ↔ [K$_4$(H$_2$L)]$^{8-}$	9.76(3)	4.61(3)	—
4 K$^+$ + H$_3$L^{11-} ↔ [K$_4$(H$_3$L)]$^{7-}$	—	4.50(5)	5.42(5)
3 K$^+$ + H$_4$L^{10-} ↔ [K$_3$(H$_4$L)]$^{7-}$	5.446(5)	3.94(4)	3.36(5)
2 K$^+$ + H$_5$L^{9-} ↔ [K$_2$(H$_5$L)]$^{7-}$	3.820(7)	2.79(7)	—
K$^+$ + H$_6$L^{8-} ↔ [K(H$_6$L)]$^{7-}$	2.58(5)	—	—
K$^+$ + H$_7$L^{7-} ↔ [K(H$_7$L)]$^{6-}$	2.08(3)	—	—
Mg^{2+} + L^{14-} + 4 K$^+$ ↔ [MgK$_4$L]$^{8-}$	22.4(1)	—	—
Mg^{2+} + HL^{13-} + 4 K$^+$ ↔ [MgK$_4$(HL)]$^{7-}$	21.6(1)	11.64(5)	—
Mg^{2+} + H$_2$L^{12-} + 3 K$^+$ ↔ [MgK$_3$(H$_2$L)]$^{7-}$	18.1(1)	9.75(7)	—
Mg^{2+} + H$_3$L^{11-} + 3 K$^+$ ↔ [MgK$_3$(H$_3$L)]$^{6-}$	15.0(1)	8.79(7)	—
Mg^{2+} + H$_4$L^{10-} + 2 K$^+$ ↔ [MgK$_2$(H$_4$L)]$^{6-}$	11.6(1)	6.96(7)	—
Mg^{2+} + H$_5$L^{9-} + K$^+$ ↔ [MgK(H$_5$L)]$^{6-}$	9.1(1)	5.26(7)	—
Mg^{2+} + H$_6$L^{8-} + K$^+$ ↔ [MgK(H$_6$L)]$^{5-}$	7.3(1)	—	—
Mg^{2+} + H$_6$L^{8-} ↔ [Mg(H$_6$L)]$^{6-}$	—	4.71(7)	—

[a] This work, σ = 0.033 (H$^+$), 0.053 (K$^+$) and 0.051 (Mg^{2+}). [b] Thermodynamic data reported previously for similar systems are included for comparison; the equations in the left column refer to InsP$_8$ complexes [28,46,47]. The standard deviation on the uncertain digit is added between brackets.

Since InsP$_8$ would never occur naturally without a background of coordinating ions, we repeated the ^{31}P-NMR titration in the presence of 150 mM K$^+$ ions (Figure 5b). Compared to the spectra recorded in solution devoid of coordination ions, all peaks were shifted downfield in the presence of K$^+$, suggesting the formation of K$^+$ complexes. Using Hyp-NMR software, the protonation constants from above, and the experimental chemical shift values in the presence of K$^+$, the formation constants and abundance of six different K$^+$ complexes of InsP$_8$ were calculated, along with the most likely sequence of protonation and complexation events (Figures 5d and S7, Table 1). The [K$_5$(HL)]$^{8-}$ complex is by far the most abundant species down to about pH 10, reflected by the almost unchanging chemical shift values. The third protonation event (from [K$_4$(H$_2$L)]$^{8-}$ to [K$_4$(H$_3$L)]$^{7-}$) coincides with the conformational change, accompanied by a steep upfield shift of all monophosphate peaks around pH 8.5–9.0, consistent with our NMR data above (Figure 3).

Around physiological pH, the most abundant complex is predicted to be [K$_2$(H$_5$L)]$^{7-}$, in which one K$^+$ ion is coordinated to phosphates in position P6, P5α and P5β. The other K$^+$ ion is coordinated to the pyrophosphate group at the 1-position, between P1α and P2 (Figure S7). Overall, K$^+$ complexes of InsP$_8$ were found to be substantially more

stable than equivalent complexes with $InsP_6$ or 5PCP-$InsP_5$ (see formation constants in Table 1). For example, the formation constant of $[K_2(H_5L)]^{7-}$, the main K^+-complex of $InsP_8$ at physiological pH, is more than tenfold higher than that of the corresponding 5PCP-$InsP_5$ complex (for a full description of all detected complexes and their analysis, see Supplementary Materials).

Finally, to more closely approximate physiological solution conditions and to include divalent cations, we recorded ^{31}P-NMR titration curves of $InsP_8$ in the presence of 150 mM KCl and 1 mM $MgCl_2$ (Figure 6a). Combined with protonation and K^+-complexation constants from the previous titrations, the formation constants and likely structures for seven K^+-Mg^{2+} complexes were calculated (Table 1 and Figure S8). Due to the propensity of $InsP_8$ to precipitate, it was not possible to add more than one equiv. $MgCl_2$. The complex described above is therefore not entirely representative of biologically relevant species, but provides some insights nonetheless. Once again, Mg^{2+}-complexes of $InsP_8$ are far more stable than the equivalent ones formed by 5PCP-$InsP_5$, as illustrated by much larger formation constants (Table 1).

The speciation diagram (Figure 6b) highlights the coexistence of several different complexes at any given pH value, especially towards lower pH. In the physiological pH range, the most abundant species is $[MgK_3(H_3L)]^{6-}$, in which the Mg^{2+} ion is coordinated by the pyrophosphate group at 1-position, together with P2 (Figure 6c,d). As for the previous titrations, transition to the equatorial conformation was indicated by a steep upfield shift of monophosphate resonances, concomitant with the third protonation step at around pH 8.5 (likely in position 6, $[K_3Mg(H_2L)]^{7-}$ to $[K_3Mg(H_3L)]^{6-}$). At pH 8.0 and 8.5, the P2 peak was too broad to detect, suggesting higher rates of exchange between conformations in the presence of one equivalent Mg^{2+}, which move the system into the intermediate exchange range even with ^{31}P-NMR detection.

The results illustrate the extremely tight association between $InsP_8$ and K^+ or Mg^{2+} ions, and suggest an important role of the two pyrophosphate groups in Mg^{2+} binding. While in the axial conformation, $InsP_8$ coordinates Mg^{2+} between its two pyrophosphate groups; once the conformation has changed to equatorial, the Mg^{2+} binding site is formed by the pyrophosphate group at position 1 and the phosphate group at position 2 (Figure 6c). These insights might inform future structural studies.

3.5. Complex Speciation of InsP₈ Affects Protein Binding

Considering how sensitively $InsP_8$ speciation reacts to solution conditions, such as pH and ionic composition, we wondered to what extent this speciation could influence the interaction of $InsP_8$ with proteins. To test this, the binding of $InsP_8$ to a known InsP-binding domain, the SPX domain (named after Syg1, Pho81, Xpr1 proteins) from yeast VTC2 [39,48] was investigated using isothermal titration calorimetry (ITC).

The first set of experiments was performed at pH 7.4 and approximately physiological salt composition, but without divalent ions. Based on our previous experiments, we expect $InsP_8$ to adopt its equatorial conformation under these conditions. A fairly strong interaction between $InsP_8$ and VTC2-SPX was observed, which could be fitted with a one-binding-site model (Figures 7a and S9a). The dissociation constant K_d was 373 nM (mean of three replicates), i.e., in the same range as previously published results for PP-InsPs binding to VTC2-SPX [39,48] or $InsP_8$ interacting with the SPX domain of human XPR1 [9]. While both enthalpic and entropic parameters were in favor of binding, the entropic contribution was the dominant one ($\Delta H = -3.5$ kcal/mol, $-T\Delta S = -5.2$ kcal/mol at 25 °C, mean of three replicates).
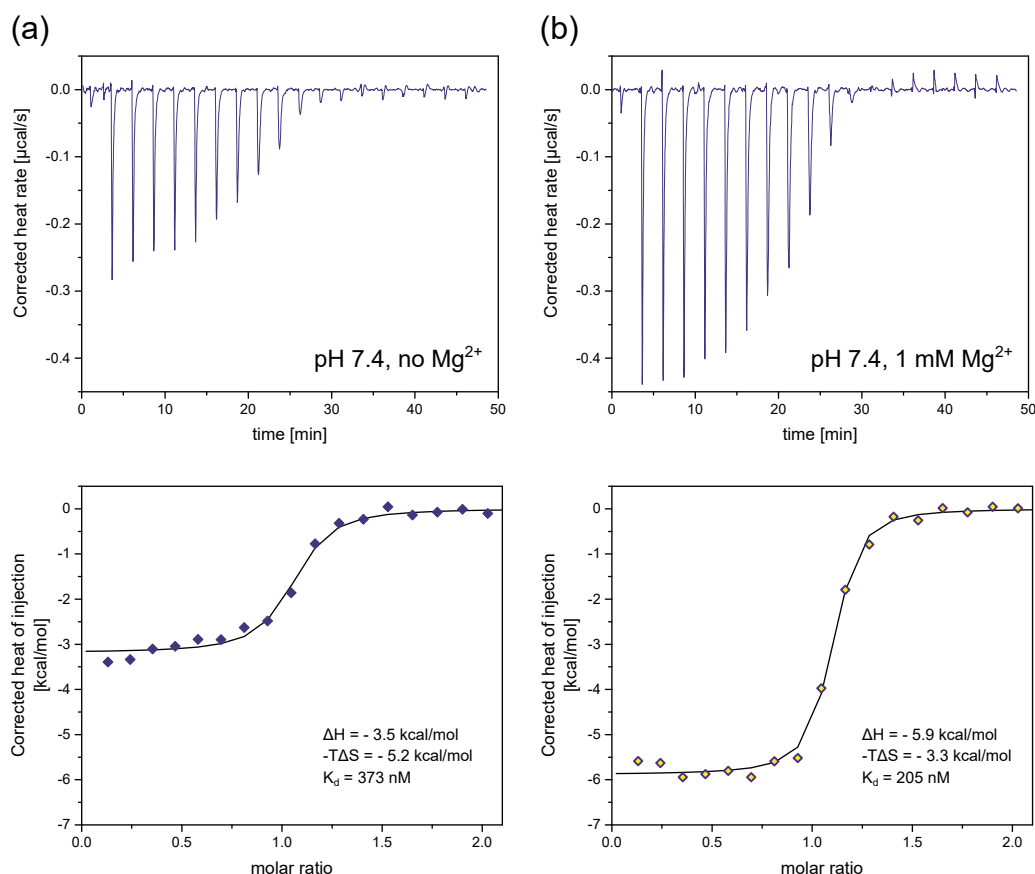
Figure 7. Isothermal titration calorimetry of (**a**) InsP$_8$ binding to the yeast VTC2 SPX–domain (50 μM) in ITC binding buffer (25 mM HEPES pH 7.4, 150 mM KCl, 40 mM NaCl, 0.5 mM TCEP) at 25 °C. (**b**) Addition of 1 mM MgCl$_2$ substantially decreases ΔH, ΔS and the binding constant K$_d$. The figure shows one representative replicate per condition, out of three replicates (Figure S9). ΔH, ΔS and K$_d$ are reported as the average of three replicates.

Next, we repeated the experiment in the presence of 1 mM MgCl$_2$, where we expected a substantial portion of InsP$_8$ to adopt the axial conformation (Figures 7b and S9b). We specifically chose assay conditions that allowed us to maintain constant pH, so it would not affect the electrostatic properties of the protein, while controlling the conformational equilibrium of InsP$_8$ through the Mg^{2+} concentration alone. We observed that ΔH, ΔS and K$_d$ all changed upon addition of MgCl$_2$. K$_d$ decreased to 205 nM (mean of three replicates). Interestingly, the enthalpy of binding became the dominant factor in the presence of MgCl$_2$; ΔH became more negative (−5.9 kcal/mol) and −TΔS less negative (−3.3 kcal/mol) on average. These results confirm the negative correlation between ΔH and −TΔS, which is typical of protein ligand interactions. Enthalpically more favorable interactions are generally less favorable in terms of entropy, with a clear correlation across diverse ligand types [49]. K$_d$ decreased notably, indicating improved binding in the presence of Mg^{2+} ions.

In summary, we found that addition of MgCl$_2$ strengthened the binding of InsP$_8$ to the VTC2 SPX-domain under approximately physiological conditions.

4. Discussion

We have conducted a systematic comparison of inositol poly- and pyrophosphates regarding their conformation at varying pH and ionic composition. Despite their structural similarities and comparable charge, clear differences between InsP$_6$, 5PP-InsP$_5$ and InsP$_8$ became apparent. Generally speaking, the more phosphoryl groups the molecules carry, the lower the pH range in which the conformational change takes place. It was previously demonstrated for InsP$_6$ that phosphoryl groups are spatially better separated in the axial

conformation, minimizing steric and electrostatic repulsion between the anionic groups and providing one of the driving forces for the conformational change of higher InsPs (Figure 1c) [26,28]. Additional phosphoryl groups lead to accumulation of more negative charge in the equatorial plane, which means a critical charge density is reached at lower pH, facilitating the conformational change.

Our results also confirmed previous studies, which demonstrated that metal cation coordination can promote the transition to the axial conformation at lower pH. Frost et al. reported as early as 1979 that alkali cations stabilize the axial conformation of $InsP_6$ [43]. There have since been multiple studies showing that complexation of various metals promotes the transition to axial $InsP_6$ [47,50–52]. Hager et al. could subsequently show that Mg^{2+} ions help to stabilize $5PCP\text{-}InsP_5$ in an axial conformation [28,43]. Notably, we now found that $InsP_8$ begins to change conformation at pH* 7.5 (=pH 7.4) in the presence of 5 equiv. $MgCl_2$—reminiscent of cytosolic conditions—which led us to focus our subsequent efforts on this molecule.

Thermodynamic studies provided more information about the conformational equilibrium of $InsP_8$. The transition from the equatorial to axial conformation is an exothermic process, and the formation of the axial conformer is enthalpically favored but entropically hindered. Addition of Mg^{2+} ions reduced both the enthalpic driving force and the entropic penalty, shifting the equilibrium more toward the axial side. As has been previously demonstrated for $InsP_6$, the phosphoryl groups are more exposed to the solvent in the axial conformation, leading to a more ordered hydration shell and overall loss of entropy compared to equatorial conformation, hence a negative ΔS [26]. Positively charged Mg^{2+} ions will coordinate to the phosphoryl groups, thereby shielding some of the negative charge, which reduces hydration, and could explain why there is less entropic penalty associated with the conformational change at higher Mg^{2+} concentrations. Similarly, coordination of Mg^{2+} cations might also reduce electrostatic repulsion between phosphoryl groups in the equatorial plane, thus reducing the enthalpic driving force towards the axial conformation. Of course, the forces governing the conformational equilibrium are likely more complex than the interpretation above. A plethora of different multinuclear complexes can be expected to coexist and interconvert, each with its own protonation/complexation/conformation equilibria. The parameters we determined experimentally should therefore be understood as the sum of all these processes.

Trying to make a prediction about $InsP_8$ in biological settings based on our results, we considered the following. Our assay conditions can only approximate cytosolic conditions, and we did not increase $MgCl_2$ content beyond 0.25 mM or five equivalents relative to 50 μM $InsP_8$, to avoid precipitation. Furthermore, the concentration of $InsP_8$ could not be reduced below 50 μM, without compromising the NMR detection. However, the endogenous concentration $InsP_8$ is thought to be around 1 μM, and cytosolic concentrations of free Mg^{2+} are approximately 0.5–1 mM [32,53]. Therefore, there is a far greater excess of Mg^{2+} in a cytosolic setting than in our assays. This excess should push the conformational equilibrium further toward the axial side than the ca. 30% we observed under our conditions. Nevertheless, five equivalents Mg^{2+} should largely saturate $InsP_8$, which at pH 7.4 carries 10–11 negative charges (Figure 5). For comparison, $InsP_6$ is also predicted to form pentamagnesium complexes under cytosolic conditions [24,46]. Taken together, these considerations strongly suggest that $InsP_8$ is actively interconverting between conformations under cytosolic conditions. Based on our experiments, we expect more than 30% of the cytosolic pool of $InsP_8$ to adopt an axial conformation under physiological conditions.

Phosphorous NMR studies revealed further details of the speciation of $InsP_8$ regarding protonation and complexation with potassium and magnesium ions. At physiological pH and in the presence of K^+ and an equimolar amount of Mg^{2+}, the most abundant species is the equatorial complex $[MgK_3(H_3L)]^{6-}$, in which Mg^{2+} is coordinated to P2, P1α and P1β. Another species present at physiological pH is the axial complex $[MgK_3(H_2L)]^{7-}$ in which Mg^{2+} is coordinated by P5α and P1α. Overall, the pyrophosphate groups in positions 1 and 5 play an essential role in Mg^{2+} binding, as the ion is always coordinated to either the

two pyrophosphate groups (in axial complexes) or P2 and PP1 (in equatorial complexes). Notably, all metal complexes of InsP$_8$ are far more stable than the equivalent ones formed by InsP$_6$ or 5PP-InsP$_5$.

The Mg^{2+} complexes of PP-InsPs were also found to be more stable than those of ATP and ADP, two other well-known cytosolic Mg^{2+} chelators. Formation constants of complexes between Mg^{2+} and ATP, previously reported at 150 mM NaCl and 37 °C [54] are: Mg^{2+} + ATP^{4-} → [MgATP]$^{2-}$: log(K) = 4.34, Mg^{2+} + HATP^{3-} → [Mg(HATP)]$^-$: log(K) = 2.39. In contrast, we measured formation constants (log(K)) of 15.0 and 8.7 for [MgK$_3$(H$_3$L)] complexes of InsP$_8$ and 5PCP-InsP$_5$. It therefore appears feasible that the significant stability of these complexes influences their interactions with other biomolecules. Do metal ions bridge binding interactions between PP-InsPs and proteins? And if so, is this effect more pronounced for InsP$_8$ than its less densely phosphorylated relatives? And how does this ultimately influence the strength and specificity of binding?

One could envision signaling functions associated with the metal complexation and the conformational equilibrium of PP-InsPs. In light of their role as cellular ATP and phosphate sensors, additional sensing functions seem plausible [8,48]. Given how sensitively PP-InsP speciation reacts to solution conditions in vitro, it is highly likely to change upon local subcellular perturbations in pH or metal composition, which may promote selective engagement of signaling partners. Such a pH-sensing mechanism has been demonstrated in the case of the yeast transcription factor Opi1, which is retained on the ER membrane by binding to phosphatidic acid (PA). Upon decrease of intracellular pH and protonation of the PA headgroup, Opi1 was released and activated its downstream target genes involved in inositol biosynthesis [55]. The authors proposed that phosphatidyl inositol lipids might sense pH through similar mechanisms, and the same might be true for soluble InsPs. Interestingly, the enzymes KCS1 and PLC1, part of the inositol pyrophosphate synthesis pathway in yeast, were found in a genome-wide screen for proteins involved in intracellular pH sensing [56].

In the large majority of cases, it is unclear by which mechanisms proteins manage to recognize and distinguish the different PP-InsPs [9,23]. Differential metal binding and/or a drastically altered molecular shape in the axial conformation might provide a convenient way to recognize the appropriate ligand. The idea that solution conditions, specifically the presence or absence of divalent cations, can have a significant influence on the outcome of in vitro binding studies with InsPs has already been proposed more than twenty years ago [57]. Our ITC experiments now provide a first hint that InsP speciation might play a role in this differentiation. Dissociation constants for InsP$_8$ binding to the VTC2 SPX domain were almost cut in half by addition of 1 mM Mg^{2+}, and binding shifted towards a more enthalpically dominated interaction in the presence of Mg^{2+}. It is tempting to speculate that the decrease in ΔH might reflect a more specific fit of an axial magnesium complex into the binding site, compared to the free, equatorial molecule, but structural evidence would be a prerequisite to support this hypothesis and is currently unavailable. Based on the current data, we cannot exclude the possibility that Mg^{2+} might lower the K$_d$ independently of InsP$_8$ conformation, for example, by altering the enthalpy and entropy of desolvation upon formation of the InsP$_8$-Mg complex. It will be interesting to investigate the influence of Mg coordination more systematically for other proteins targeted by PP-InsPs, such as the mammalian SPX domain of XPR1, or the C2 domains of synaptotagmin isoforms.

Overall, our results highlight the immense complexity of PP-InsP speciation and how this speciation may influence their behavior. Solution conditions for PP-InsP-protein binding experiments in the literature differ widely regarding pH, salts, and other additives. For future biochemical studies, it will be important to consider carefully which molecular species are formed under the given assay conditions, how those conditions might affect the experimental outcome, and to what extent the conditions mirror cellular settings. An accurate understanding of this complexity will be indispensable in decoding the diverse roles of InsPs and PP-InsPs as cellular messengers.

References

1. Chatree, S.; Thongmaen, N.; Tantivejkul, K.; Sitticharoon, C.; Vucenik, I. Role of Inositols and Inositol Phosphates in Energy Metabolism. *Molecules* **2020**, *25*, 5079. [CrossRef]
2. Shears, S.B. Inositol Pyrophosphates: Why so Many Phosphates? *Adv. Biol. Regul.* **2015**, *57*, 203–216. [CrossRef]
3. Nguyen Trung, M.; Furkert, D.; Fiedler, D. Versatile Signaling Mechanisms of Inositol Pyrophosphates. *Curr. Opin. Chem. Biol.* **2022**, *70*, 102177. [CrossRef]
4. Gu, C.; Nguyen, H.N.; Hofer, A.; Jessen, H.J.; Dai, X.; Wang, H.; Shears, S.B. The Significance of the Bifunctional Kinase/Phosphatase Activities of Diphosphoinositol Pentakisphosphate Kinases (PPIP5Ks) for Coupling Inositol Pyrophosphate Cell Signaling to Cellular Phosphate Homeostasis. *J. Biol. Chem.* **2017**, *292*, 4544–4555. [CrossRef]
5. Benjamin, B.; Garg, A.; Jork, N.; Jessen, H.J.; Schwer, B.; Shuman, S. Activities and Structure-Function Analysis of Fission Yeast Inositol Pyrophosphate (IPP) Kinase-Pyrophosphatase Asp1 and Its Impact on Regulation of Pho1 Gene Expression. *MBio* **2022**, *13*, e0103422. [CrossRef]
6. Pascual-Ortiz, M.; Walla, E.; Fleig, U.; Saiardi, A. The PPIP5K Family Member Asp1 Controls Inorganic Polyphosphate Metabolism in S. Pombe. *J. Fungi* **2021**, *7*, 626. [CrossRef]
7. Zhu, J.; Lau, K.; Puschmann, R.; Harmel, R.K.; Zhang, Y.; Pries, V.; Gaugler, P.; Broger, L.; Dutta, A.K.; Jessen, H.J.; et al. Two Bifunctional Inositol Pyrophosphate Kinases/Phosphatases Control Plant Phosphate Homeostasis. *Elife* **2019**, *8*, e43582. [CrossRef]
8. Dong, J.; Ma, G.; Sui, L.; Wei, M.; Satheesh, V.; Zhang, R.; Ge, S.; Li, J.; Zhang, T.E.; Wittwer, C.; et al. Inositol Pyrophosphate InsP8 Acts as an Intracellular Phosphate Signal in Arabidopsis. *Mol. Plant* **2019**, *12*, 1463–1473. [CrossRef]
9. Li, X.; Gu, C.; Hostachy, S.; Sahu, S.; Wittwer, C.; Jessen, H.J.; Fiedler, D.; Wang, H.; Shears, S.B. Control of XPR1-Dependent Cellular Phosphate Efflux by InsP8 Is an Exemplar for Functionally-Exclusive Inositol Pyrophosphate Signaling. *Proc. Natl. Acad. Sci. USA* **2020**, *117*, 3568–3574. [CrossRef]
10. Wilson, M.S.; Jessen, H.J.; Saiardi, A. The Inositol Hexakisphosphate Kinases IP6K1 and -2 Regulate Human Cellular Phosphate Homeostasis, Including XPR1-Mediated Phosphate Export. *J. Biol. Chem.* **2019**, *294*, 11597–11608. [CrossRef]
11. Legati, A.; Giovannini, D.; Nicolas, G.; López-Sánchez, U.; Quintáns, B.; Oliveira, J.R.M.; Sears, R.L.; Ramos, E.M.; Spiteri, E.; Sobrido, M.-J.; et al. Mutations in XPR1 Cause Primary Familial Brain Calcification Associated with Altered Phosphate Export. *Nat. Genet.* **2015**, *47*, 579–581. [CrossRef]
12. Yousaf, R.; Gu, C.; Ahmed, Z.M.; Khan, S.N.; Friedman, T.B.; Riazuddin, S.; Shears, S.B.; Riazuddin, S. Mutations in Diphosphoinositol-Pentakisphosphate Kinase PPIP5K2 Are Associated with Hearing Loss in Human and Mouse. *PLoS Genet.* **2018**, *14*, e1007897. [CrossRef]
13. Khaled, M.L.; Bykhovskaya, Y.; Gu, C.; Liu, A.; Drewry, M.D.; Chen, Z.; Mysona, B.A.; Parker, E.; McNabb, R.P.; Yu, H.; et al. PPIP5K2 and PCSK1 Are Candidate Genetic Contributors to Familial Keratoconus. *Sci. Rep.* **2019**, *9*, 19406. [CrossRef]
14. Szijgyarto, Z.; Garedew, A.; Azevedo, C.; Saiardi, A. Influence of Inositol Pyrophosphates on Cellular Energy Dynamics. *Science* **2011**, *334*, 802–805. [CrossRef]

15. Qin, N.; Li, L.; Ji, X.; Pereira, R.; Chen, Y.; Yin, S.; Li, C.; Wan, X.; Qiu, D.; Jiang, J.; et al. Flux Regulation through Glycolysis and Respiration Is Balanced by Inositol Pyrophosphates in Yeast. *Cell* **2023**, *186*, 748–763.e15. [CrossRef]

16. Illies, C.; Gromada, J.; Fiume, R.; Leibiger, B.; Yu, J.; Juhl, K.; Yang, S.-N.; Barma, D.K.; Falck, J.R.; Saiardi, A.; et al. Requirement of Inositol Pyrophosphates for Full Exocytotic Capacity in Pancreatic b Cells. *Science* **2007**, *318*, 1299–1302. [CrossRef]

17. Zhang, X.; Li, N.; Zhang, J.; Zhang, Y.; Yang, X.; Luo, Y.; Zhang, B.; Xu, Z.; Zhu, Z.; Yang, X.; et al. 5-IP7 Is a GPCR Messenger Mediating Neural Control of Synaptotagmin-Dependent Insulin Exocytosis and Glucose Homeostasis. *Nat. Metab.* **2021**, *3*, 1400–1414. [CrossRef]

18. Chakraborty, A.; Koldobskiy, M.A.; Bello, N.T.; Maxwell, M.; Potter, J.J.; Juluri, K.R.; Maag, D.; Kim, S.; Huang, A.S.; Dailey, M.J.; et al. Inositol Pyrophosphates Inhibit Akt Signaling, Thereby Regulating Insulin Sensitivity and Weight Gain. *Cell* **2010**, *143*, 897–910. [CrossRef]

19. Pavlovic, I.; Thakor, D.T.; Vargas, J.R.; McKinlay, C.J.; Hauke, S.; Anstaett, P.; Camunã, R.C.; Bigler, L.; Gasser, G.; Schultz, C.; et al. Cellular Delivery and Photochemical Release of a Caged Inositol-Pyrophosphate Induces PH-Domain Translocation in Cellulo. *Nat. Commun.* **2016**, *7*, 10622. [CrossRef]

20. Zhang, Z.; Zhao, C.; Liu, B.; Liang, D.; Qin, X.; Li, X.; Zhang, R.; Li, C.; Wang, H.; Sun, D.; et al. Inositol Pyrophosphates Mediate the Effects of Aging on Bone Marrow Mesenchymal Stem Cells by Inhibiting Akt Signaling. *Stem Cell Res. Ther.* **2014**, *5*, 33. [CrossRef]

21. Zhu, Q.; Ghoshal, S.; Rodrigues, A.; Gao, S.; Asterian, A.; Kamenecka, T.M.; Barrow, J.C.; Chakraborty, A. Adipocyte-Specific Deletion of Ip6k1 Reduces Diet-Induced Obesity by Enhancing AMPK-Mediated Thermogenesis. *J. Clin. Investig.* **2016**, *126*, 4273–4288. [CrossRef]

22. Moritoh, Y.; Abe, S.-I.; Akiyama, H.; Kobayashi, A.; Koyama, R.; Hara, R.; Kasai, S.; Watanabe, M. The Enzymatic Activity of Inositol Hexakisphosphate Kinase Controls Circulating Phosphate in Mammals. *Nat. Commun.* **2021**, *12*, 4847. [CrossRef]

23. Gerasimaite, R.; Pavlovic, I.; Capolicchio, S.; Hofer, A.; Schmidt, A.; Jessen, H.J.; Mayer, A. Inositol Pyrophosphate Specificity of the SPX-Dependent Polyphosphate Polymerase VTC. *ACS Chem. Biol.* **2017**, *12*, 648–653. [CrossRef]

24. Veiga, N.; Torres, J.; Godage, H.Y.; Riley, A.M.; Domínguez, S.; Potter, B.V.L.; Díaz, A.; Kremer, C. The Behaviour of Inositol 1,3,4,5,6-Pentakisphosphate in the Presence of the Major Biological Metal Cations. *J. Biol. Inorg. Chem.* **2009**, *14*, 1001–1013. [CrossRef]

25. Veiga, N.; Torres, J.; Cerdá, F.; González, G.; Gómez, K.; Mansell, D.; Freeman, S.; Domínguez, S.; Kremer, C. Redox and Structural Aspects on Iron Inositol 1,2,3-Trisphosphate Interaction: An Experimental and Computational Approach. *J. Mol. Struct.* **2011**, *994*, 343–349. [CrossRef]

26. Veiga, N.; Torres, J.; MacHo, I.; Gómez, K.; González, G.; Kremer, C. Coordination, Microprotonation Equilibria and Conformational Changes of Myo-Inositol Hexakisphosphate with Pertinence to Its Biological Function. *Dalt. Trans.* **2014**, *43*, 16238–16251. [CrossRef]

27. Riley, A.M.; Trusselle, M.; Kuad, P.; Borkovec, M.; Cho, J.; Choi, J.H.; Qian, X.; Shears, S.B.; Spiess, B.; Potter, B.V.L. Scyllo-Inositol Pentakisphosphate as an Analogue of Myo-Inositol 1,3,4,5,6-Pentakisphosphate: Chemical Synthesis, Physicochemistry and Biological Applications. *ChemBioChem* **2006**, *7*, 1114–1122. [CrossRef]

28. Hager, A.; Wu, M.; Wang, H.; Brown, N.W.J.; Shears, S.B.; Veiga, N.; Fiedler, D. Cellular Cations Control Conformational Switching of Inositol Pyrophosphate Analogues. *Chemistry* **2016**, *22*, 12406–12414. [CrossRef]

29. Barker, C.J.; Wright, J.; Hughes, P.J.; Kirk, C.J.; Michell, R.H. Complex Changes in Cellular Inositol Phosphate Complement Accompany Transit through the Cell Cycle. *Biochem. J.* **2004**, *380*, 465–473. [CrossRef]

30. Harmel, R.K.; Puschmann, R.; Nguyen Trung, M.; Saiardi, A.; Schmieder, P.; Fiedler, D. Harnessing (13)C-Labeled Myo-Inositol to Interrogate Inositol Phosphate Messengers by NMR. *Chem. Sci.* **2019**, *10*, 5267–5274. [CrossRef]

31. Qiu, D.; Wilson, M.S.; Eisenbeis, V.B.; Harmel, R.K.; Riemer, E.; Haas, T.M.; Wittwer, C.; Jork, N.; Gu, C.; Shears, S.B.; et al. Analysis of Inositol Phosphate Metabolism by Capillary Electrophoresis Electrospray Ionization Mass Spectrometry. *Nat. Commun.* **2020**, *11*, 6035. [CrossRef]

32. Gu, C.; Wilson, M.S.C.; Jessen, H.J.; Saiardi, A.; Shears, S.B. Inositol Pyrophosphate Profiling of Two HCT116 Cell Lines Uncovers Variation in InsP8 Levels. *PLoS ONE* **2016**, *11*, e0165286. [CrossRef]

33. Puschmann, R.; Harmel, R.K.; Fiedler, D. Scalable Chemoenzymatic Synthesis of Inositol Pyrophosphates. *Biochemistry* **2019**, *58*, 3927–3932. [CrossRef]

34. Findeisen, M.; Berger, T.; Berger, S. A ^{1}H-NMR Thermometer Suitable for Cryoprobes.Pdf. *Magn. Reson. Chem.* **2007**, *45*, 175–178. [CrossRef]

35. Kręzel, A.; Bal, W. A Formula for Correlating PKa Values Determined in D 2O and H2O. *J. Inorg. Biochem.* **2004**, *98*, 161–166. [CrossRef]

36. Frassineti, C.; Ghelli, S. NMR as a Tool for Determining Protonation Constants of Nutral Polyprotic Bases in Solution. *Anal. Biochem.* **1995**, *231*, 374–382. [CrossRef]

37. Gans, P.; Sabatini, A.; Vacca, A. Investigation of Equilibria in Solution. Determination of Equilibrium Constants with the HYPERQUAD Suite of Programs. *Talanta* **1996**, *43*, 1739–1753. [CrossRef]

38. Alderighi, L.; Gans, P.; Ienco, A.; Peters, D.; Sabatini, A.; Vacca, A. Hyperquad Simulation and Speciation (HySS): A Utility Program for the Investigation of Equilibria Involving Soluble and Partially Soluble Species. *Coord. Chem. Rev.* **1999**, *184*, 311–318. [CrossRef]

39. Couto, D.; Richter, A.; Walter, H.; Furkert, D.; Hothorn, M.; Fiedler, D. Using Biotinylated Myo -Inositol Hexakisphosphate to Investigate Inositol Pyrophosphate—Protein Interactions with Surface-Based Biosensors. *Biochemistry* **2021**, *60*, 2739–2748. [CrossRef]

40. Frisch, M.J.; Trucks, G.W.; Schlegel, H.B.; Scuseria, G.E.; Robb, M.A.; Cheeseman, J.R.; Scalmani, G.; Barone, V.; Petersson, G.A.; Nakatsuji, H.; et al. *Gaussian 09, Revision A.02*; Gaussian, Inc.: Wallingford, CT, USA, 2016.

41. Hay, P.J.; Wadt, W.R. Ab Initio Effective Core Potentials for Molecular Calculations. Potentials for K to Au Including the Outermost Core Orbitale. *J. Chem. Phys.* **1985**, *82*, 299–310. [CrossRef]

42. Marenich, A.V.; Cramer, C.J.; Truhlar, D.G. Universal Solvation Model Based on Solute Electron Density and on a Continuum Model of the Solvent Defined by the Bulk Dielectric Constant and Atomic Surface Tensions. *J. Phys. Chem. B* **2009**, *113*, 6378–6396. [CrossRef]

43. Frost, E.B. Conformational States of Myo-Inositol Hexakisphosphate in Aqueous Solution. A 13C NMR, 31P NMR, and Raman Spectroscopic Investigation. *Science* **1979**, *47*, 416–417. [CrossRef]

44. Barrientos, L.G.; Murthy, P.P.N. Conformational Studies of Myo-Inositol Phosphates. *Carbohydr. Res.* **1996**, *296*, 39–54. [CrossRef]

45. Veiga, N.; Torres, J.; Macho, I.; Gómez, K.; Godage, H.Y.; Riley, A.M.; Potter, B.V.L.; González, G.; Kremer, C. Inframolecular Acid–Base and Coordination Properties towards Na$^+$ and Mg^{2+} of Myo-Inositol 1,3,4,5,6-Pentakisphosphate: A Structural Approach to Biologically Relevant Species. *J. Chem. Soc. Dalt. Trans.* **2013**, *42*, 6021–6032. [CrossRef]

46. Torres, J.; Domínguez, S.; Cerdá, M.F.; Obal, G.; Mederos, A.; Irvine, R.F.; Díaz, A.; Kremer, C. Solution Behaviour of Myo-Inositol Hexakisphosphate in the Presence of Multivalent Cations. Prediction of a Neutral Pentamagnesium Species under Cytosolic/Nuclear Conditions. *J. Inorg. Biochem.* **2005**, *99*, 828–840. [CrossRef]

47. Torres, J.; Veiga, N.; Gancheff, J.S.; Domínguez, S.; Mederos, A.; Sundberg, M.; Sánchez, A.; Castiglioni, J.; Díaz, A.; Kremer, C. Interaction of Myo-Inositol Hexakisphosphate with Alkali and Alkaline Earth Metal Ions: Spectroscopic, Potentiometric and Theoretical Studies. *J. Mol. Struct.* **2008**, *874*, 77–88. [CrossRef]

48. Wild, R.; Gerasimaite, R.; Jung, J.-Y.; Truffault, V.; Pavlovic, I.; Schmidt, A.; Saiardi, A.; Jessen, H.J.; Poirier, Y.; Hothorn, M.; et al. Control of Eukaryotic Phosphate Homeostasis by Inositol Polyphosphate Sensor Domains. *Science* **2016**, *352*, 986–990. [CrossRef]

49. Reynolds, C.H.; Holloway, M.K. Thermodynamics of Ligand Binding and Efficiency. *ACS Med. Chem. Lett.* **2011**, *2*, 433–437. [CrossRef]

50. Šala, M.; Makuc, D.; Kolar, J.; Plavec, J.; Pihlar, B. Potentiometric and 31P NMR Studies on Inositol Phosphates and Their Interaction with Iron(III) Ions. *Carbohydr. Res.* **2011**, *346*, 488–494. [CrossRef]

51. Veiga, N.; Macho, I.; Gómez, K.; González, G.; Kremer, C.; Torres, J. Potentiometric and Spectroscopic Study of the Interaction of 3d Transition Metal Ions with Inositol Hexakisphosphate. *J. Mol. Struct.* **2015**, *1098*, 55–65. [CrossRef]

52. Asensio, G.; Hernández-Arriaga, A.M.; Martín del Campo, M.; Prieto, A.M.; Rojo, L.; Vázquez-Lasa, B. A Study on Sr/Zn Phytate Complexes: Structural Properties and Antimicrobial Synergistic Effects against Streptococcus Mutans. *Sci. Rep.* **2022**, *12*, 20177. [CrossRef]

53. Romani, A.M.P. Intracellular Magnesium Homeostasis. *Arch. Biochem. Biophys.* **2011**, *512*, 13–58. [CrossRef]

54. Smith, R.M.; Martell, A.E.; Chen, Y. Critical Evaluation of Stability Constants for Nucleotide Complexes with Protons and Metal Ions and the Accompanying Enthalpy Changes. *Pure Appl. Chem.* **1991**, *63*, 1015–1080. [CrossRef]

55. Young, B.P.; Shin, J.J.H.; Orij, R.; Chao, J.T.; Li, S.C.; Guan, X.L.; Loewen, C.J.R. Phosphatidic Acid Is a PH Biosensor That Links Membrane Biogenesis to Metabolism. *Science* **2010**, *329*, 1085–1088. [CrossRef]

56. Orij, R.; Urbanus, M.L.; Vizeacoumar, F.J.; Giaever, G.; Boone, C.; Nislow, C.; Brul, S.; Smits, G.J. Genome-Wide Analysis of Intracellular PH Reveals Quantitative Control of Cell Division Rate by PH(c) in Saccharomyces Cerevisiae. *Genome Biol.* **2012**, *13*, R80. [CrossRef]

57. Shears, S.B. Assessing the Omnipotence of Inositol Hexakisphosphate. *Cell. Signal.* **2001**, *13*, 151–158. [CrossRef]

58. Moedritzer, K. PH Dependence of Phosphorus-31 Chemical Shifts and Coupling Constants of Some Oxyacids of Phosphorus. *Inorg. Chem.* **1967**, *6*, 936–939. [CrossRef]